Class of tunable wide band gap semiconductors γ-$(Ge_xSi_{1-x})_3N_4$

T. D. Boyko,[1,*] E. Bailey,[2] A. Moewes,[1] and P. F. McMillan[2]
[1]*Department of Physics and Engineering Physics, University of Saskatchewan, 116 Science Place, Saskatoon, Saskatchewan, Canada S7N 5E2*
[2]*Department of Chemistry, University College London, 20 Gordon Street, London WC1H 0AJ, United Kingdom*
(Received 18 January 2010; revised manuscript received 29 March 2010; published 16 April 2010)

The solid solutions of γ-Si_3N_4 and γ-Ge_3N_4, γ-$(Ge_xSi_{1-x})_3N_4$ with $x=0.000$, 0.178, 0.347, 0.524, 0.875, and 1.000, are studied. The band gap values of the solid solutions measured with soft x-ray spectroscopy have a range of $3.50-5.00\pm0.20$ eV. The hardness values of these solid solutions estimated using an empirical relationship have a range of 22.2–36.0 GPa. We use the generalized gradient approximation of Perdew-Ernzerhof-Burke (GGA-PDE) within density functional theory and obtained a calculated band gap value range of 2.20–3.56 eV. The simulated N absorption and emission spectra agree very well with our measurements and the compositional trend among the calculated band gap values corresponds well with the measured values. The agreement between experimental and theoretical spectra indicates that Ge prefers the site with tetrahedral bonding symmetry. The band gap and hardness estimates have two approximately linear regimes, when $0\leq x\leq 1/3$ and $1/3\leq x\leq 1$. The band gap decreases as Ge replaces Si on octahedral sites and this suggests that the type of cation in the octahedral sites is mainly responsible for decreasing the band gap in these spinel nitrides. Our results indicate that solid solutions of γ-$(Ge_xSi_{1-x})_3N_4$ provide a class of semiconductors with a tunable wide band gap suitable for UV laser or LED applications.

DOI: 10.1103/PhysRevB.81.155207 PACS number(s): 71.20.Nr, 78.70.Dm, 78.70.En, 71.15.Mb

I. INTRODUCTION

Silicon nitride is a ceramic semiconductor that is widely used in industry. The industrial applications of this material include gas turbine engines, diesel engines and industrial heat exchangers.[1] Silicon nitrides have many desirable mechanical and chemical properties such as high strength at high temperature, good thermal stress resistance and extreme resistance to surface oxidation. Ceramics dissociate rather than melt at high temperatures (greater than 1400 °C)[1] and typically have low thermal expansion coefficients giving them an advantage over conventional metallic alloys. Silicon nitride ceramics also have a lower mass density (40% less than conventional alloys) reducing component weight and moments of inertia.[1] These collective properties allow an increase in operating temperature, reducing the necessary cooling. This in turn increases the efficiency of devices that employ these materials. Beta silicon nitride (β-Si_3N_4) is a low-pressure hexagonal phase nitride ceramic. Gamma silicon nitride (γ-Si_3N_4) and gamma germanium nitride (γ-Ge_3N_4) are newly synthesized high-pressure spinel phase nitride ceramics.[2,3] The Si or Ge cations in these spinel materials adopt octahedral coordination presenting a unique structure that has never been seen before in binary nitride ceramics. γ-Si_3N_4 has a reduced band gap (3.6 eV) (Ref. 4) and an increased hardness (36 GPa) (Ref. 5) in comparison to β-Si_3N_4 making the hardness of γ-Si_3N_4 comparable to stishovite.[2] The increased hardness improves the quality of mechanical coatings for high temperature cutting tools[6] and the reduced band gap allows these materials to be used for optoelectronic applications including UV LEDs and lasers.[6] Studies have been carried out examining the band gap and hardness of γ-Si_3N_4 and γ-Ge_3N_4, but further characterization is necessary to allow these materials to become as widely used as their hexagonal predecessors.

The band gap is arguably one of the more important parameters when characterizing a semiconductor. The calculated band gaps of the spinel phases nitrides are reduced by as much as 33% for γ-Si_3N_4 and 10% for γ-Ge_3N_4 in comparison with their hexagonal phases nitrides (see Table I). The calculated band gap of the ternary spinel phase nitride (γ-$GeSi_2N_4$) is increased significantly (50%) from the pure germanium nitride spinel but is decreased only slightly (4%) from the pure silicon nitride spinel. The range of the theoretical band gap values is 2–4 eV and calculations suggest that the band gap of the solid solutions of these materials may be tuned in a linear fashion[2,7,8] by systematically varying the mole fraction of Ge in the final product. The band gap is also predicted to be direct in γ-Si_3N_4, γ-$GeSi_2N_4$ and γ-Ge_3N_4 allowing the possibility for optical applications in the UV regime (see Table I), such as photocatalysts used to split water.[9] The spinel nitride solid solutions are therefore excellent candidates for a new class of wide band gap semiconductors with tunable direct band gaps.

Spinel nitride ceramics not only have a small direct band gap in the UV regime, but also offer large hardness values that are highly desirable for mechanical applications. The density and hardness of the binary spinel nitrides are significantly increased in comparison to their hexagonal phase. The mass density of γ-Si_3N_4 and γ-Ge_3N_4 is increased by 23% and 20%, respectively. The increase in density is followed by an increase in the calculated (measured) bulk modulus of 11% (14%) and 30% (35%) for γ-Si_3N_4 and γ-Ge_3N_4, respectively. The calculated hardness of γ-Si_3N_4 is increased by 50% over β-Si_3N_4, while the calculated hardness of γ-Ge_3N_4 is approximately the same as β-Si_3N_4. The hardness of the ternary spinel (γ-$GeSi_2N_4$) is increased significantly from the pure germanium spinel but is only decreased slightly from pure silicon nitride. Gilman[10] proposes that there is a linear correlation between the bond modulus (in terms of molecular volume V_m and the band gap E_g) and

TABLE I. The most recently determined bulk modulus (B_0), shear modulus (G_0), Vicker's hardness (H_v), and band gap (E_g) values are displayed. The experimentally determined values are labeled with an asterisk (*), while all other values were calculated using the local density approximation (LDA). The values that have not yet been determined are indicated with a dash (—). The shear modulus labeled with *a* was determined to the be lower limit and is most likely a larger value, while the hardness indicated by *b* has a range which depended on the oxygen content. Furthermore, the type of band gap transition is labeled with (*d*) and (*i*) indicating direct or indirect, respectively.

Material	ρ (g/cm^3)	B_0 (GPa)	G_0 (GPa)	H_v (GPa)	E_g (eV)
β-Si_3N_4	3.20[a]	274[b]	112[c]	20[c]	5.18^i [d]
		270*[e]	116*[f]	30*[g]	4.8* [h]
β-Ge_3N_4	5.28[i]	185[j]			2.45^i [j]
		185*[k]			
γ-Si_3N_4	3.93[a]	305[l]	258[m]	30[m]	3.45^d [n]
		308*[l]	148*^{a}[o]	30–43*^{b}[o]	3.6* [h]
γ-$GeSi_2N_4$	4.79[n]	283[m]	231[m]	28[m]	3.3^d [m]
γ-Ge_3N_4	6.36[i]	242[m]	176[m]	18[m]	2.2^d [n]
		296*[p]			

[a]Reference 2.
[b]Reference 11.
[c]Reference 12.
[d]Reference 13.
[e]Reference 14.
[f]Reference 15.
[g]Reference 16.
[h]Reference 4.
[i]Reference 3.
[j]Reference 8.
[k]Reference 17.
[l]Reference 18.
[m]Reference 7.
[n]Reference 19.
[o]Reference 5.
[p]Reference 20.

hardness (H_v). The relationship ($H_v[\mathrm{GPa}]=C\frac{E_g}{V_m}$) indicates there is a strong correlation between hardness, structure and the band gap. Therefore, it may be possible to tailor the hardness of these materials to suit an application by tuning the band gap appropriately. The solid solutions of spinel-phase silicon nitride and germanium nitride present excellent candidates for a new class of materials with a tunable band gap and hardness. The large range of the band gap and hardness of these materials requires that reliable experimental measurements of the binary nitrides, ternary nitrides and their solid solutions be conducted to determine band gap and hardness tunability.

γ-Si_3N_4 and γ-Ge_3N_4 have the same crystal structure as all spinel structured group IV binary nitrides. The space group is *Fd*-3*m*, where cations (Ge or Si) occupy the 8*a* (tetrahedral) and 16*d* (octahedral) Wyckoff sites, while anions (N) occupy the 32*e* (tetrahedral) Wyckoff site.[21] The cations of spinel nitrides (Ge or Si) occupy both tetrahedral and octahedral coordination and have an occupancy ratio of 1:2 in the binary spinel nitride materials. Theoretical[7] and experimental[21] results both suggest Ge atoms prefer to occupy tetrahedral sites, while Si atoms prefer to occupy octahedral sites. This means that the available Ge atoms form tetrahedral bonds with N atoms before any octahedral bonds are formed and vice versa for Si atoms. In the solid solutions [γ-$(Ge_xSi_{1-x})_3N_4$]. Ge atoms occupy only tetrahedral sites while Si atoms occupy both tetrahedral and octahedral sites when $x<1/3$. When $x>1/3$, Ge atoms occupy both octahedral and tetrahedral sites, while Si atoms occupy only octahedral sites. The special case when $x=1/3$ produces the stable intermediate phase γ-$GeSi_2N_4$, where all Ge atoms occupy tetrahedral sites and all Si atoms occupy octahedral sites.[7] The three stable spinel nitride phases (γ-$GeSi_2N_4$, γ-Si_3N_4, and γ-Ge_3N_4) along with their intermediate solid solutions phases have varied bonding and structural configurations that may provide useful tunable electronic and mechanical properties.

Here we calculate the electronic structure of the solid solution phases (γ-$(Si,Ge)_3N_4$) including end members (γ-$GeSi_2N_4$ and γ-Ge_3N_4) and compare the results with X-ray emission and absorption measurements on laboratory-synthesized samples. The empirical relationship between the band gap and hardness proposed by Gilman[10] is also used to estimate the hardness of the intermediate solid solutions. The combination of these measurements and calculations is used to predict the hardness and band gap of the solid solutions for the first time.

II. EXPERIMENTAL DETAILS

Soft x-ray spectroscopy (SXS) utilizing synchrotron radiation from modern third generation sources is a powerful tool for probing the electronic structure of materials. The two complementary techniques employed here are x-ray absorption near edge spectroscopy (XANES), and x-ray emission spectroscopy (XES). In general, XANES and XES measure-

ments probe the unoccupied and occupied density of states (DOS), respectively, but there are limitations that can be advantageous to the experimentalist. Photons have angular momentum $\ell=1$. In the soft x-ray regime, photons are described accurately by the electric dipole approximation, so electronic transitions powered by the absorption of soft x-ray photons are restricted to dipole transitions ($\Delta\ell=\pm1$). The binding energies of the electrons are characteristic for each element and the probability of exciting a core electron is very large when the energy of the incident photon is tuned to the binding energy of the electron. The measurements presented here are the N Kα XES and N 1*s* XANES spectra. During these measurements the N *p*-states are probed by exciting the N 1*s* core electrons into the conduction band (XANES) or by measuring the refilling of the N 1*s* core hole by valence electrons (XES). In summary XANES and XES measurements probe the local partial density of states or LPDOS in an element specific fashion.

During a XANES measurement an x-ray photon is absorbed and the energy is used to promote a core electron into a previously unoccupied conduction band state. This is followed by another electron transition during which a valence electron decays to fill the previously created core hole. A photon can be emitted and counted as a function of excitation energy with the intensity proportional to the unoccupied DOS. The XANES spectra are measured with a non energy-dispersive channeltron fluorescence detector. This method of detection is known as total fluorescence yield (TFY). During an XES measurement a core hole is excited out of the sample (photoionzed) and the system is left in an excited state. This proceeds with a valence band electron refilling the core hole and the energy can be released in the form of a fluorescence photon. The XES spectra are measured with a high-resolution wavelength dispersive grating spectrometer. The rate at which photons are emitted at a given energy is proportional to the occupied DOS.

The materials studied here are solid solutions established between the end members γ-Si_3N_4 and γ-Ge_3N_4. Samples of γ-Si_3N_4 and γ-$(Si,Ge)_3N_4$ solid solutions were synthesized in a resistively heated multianvil press using COMPRES 8/3 MgO assemblies with a $LaCrO_3$ furnace at 1500 °C and $P=23$ GPa for 18–35 min. The pure γ-Ge_3N_4 end member was prepared at 12 GPa and 1200 °C for 2 h using a COMPRES 14/8 MgO assembly with a graphite furnace. All samples were fully characterized using x-ray diffraction, Raman spectroscopy and electron microprobe analysis in a previous study.[21] Further details of the synthesis and analysis procedures are described therein. The stoichiometry of the samples studied is γ-$(Ge_xSi_{1-x})_3N_4$ with $x=0.000$, 0.178, 0.347, 0.524, 0.875, and 1.000. The SGM beamline[22] (Canadian Light Source, Canada) and Beamline 8.0.1[23] (Advanced Light Source, USA) were utilized to collect N 1*s* XANES and N Kα XES data, respectively. The solid solution samples formed small polycrystalline pieces (<1 mm) embedded in epoxy. These were pressed onto carbon tape and placed 30 deg off normal with respect to the incident beam. Powdered samples of the pure end members, γ-Si_3N_4 and γ-Ge_3N_4, were likewise pressed onto carbon tape. The N 1*s* XANES (measured in TFY mode) and Kα XES were calibrated against the reference spectra of *h*-BN. The XES and XANES peaks for *h*-BN nearest the band gap are taken to be 394.4 and 402.1 eV.

III. THEORETICAL DETAILS

The experimental spectra are always subject to inherent experimental and lifetime broadening, there are three different mechanisms of broadening that are unavoidable. First, the core hole of the systems exists for a very short time, which creates an uncertainty in the energy of the photon emitted when the hole is refilled. The lifetime of the core hole is constant for XANES measurements and can be simulated using a Lorentzian broadening function[24] with a constant full width at half maximum (FWHM). The lifetime of the final state of the system is very short also and adds additional broadening to the spectrum for similar reasons. The lifetime of the final state depends largely upon the conduction band state to which the core electron has transitioned. Electrons in higher conduction band states may decay very quickly to lower states within the same band before the core hole is refilled, introducing uncertainty into the final state energy. This creates a variable broadening in the spectrum and is simulated using a Lorentz function[25] with a variable FWHM. Lastly, the spectrum is broadened by the finite spectral resolution of the instruments (the monochromator in XANES and the fluorescence spectrometer for XES measurements). This broadening is simulated using a Gaussian function with a variable FWHM determined by the nominal beamline resolution. In conclusion, all three broadening factors contribute in the same order of magnitude and have to be taken into account for successful simulation of measured XES and XANES spectra.

In solid crystalline materials XES and XANES probe the valence band (VB) and the conduction band (CB) states, respectively. The direct band gap is defined as the minimum energy separation between the VB and CB for the crystal. The energy separation between the XES and XANES spectra is then used to determine the band gap. There are three important considerations when using SXS to determine the band gap. The first consideration is the core hole effect.[26] XES and XANES transitions are considered one-step processes and are subject to the final state rule, which specifies that the final state electron configuration in each process is the most important.[27] In a strict one-electron picture, the final state of a XANES measurement contains a localized core hole and a delocalized electron residing in the conduction band. The final state of an XES measurement contains no core hole, but a delocalized hole resides in the valence band. The effect of the core hole only needs to be taken into account in XANES measurements. The core hole affects the measured spectra by distorting the CB such that the unoccupied LPDOS have large resonance features near the Fermi level.[28] The core hole also can shift the CB states in energy and this effectively reduces the measured band gap.

Second, one needs to consider nonequivalent sites that may have different core level binding energies. The binding energy of the core electrons is determined by the bonding characteristics and differs for nonequivalent crystal lattice sites. The XES and XANES spectra are measured relative to

the core electron's binding energy and measuring a material with two or more nonequivalent sites will produces a spectrum that is a sum of the individual site spectra shifted with respect to the binding energy of each site. The splitting of the spectral contributions effectively decreases the measured band gap since spectra from nonequivalent sites with a larger binding energy are shifted to higher energy in both the XANES and XES spectra. These values are unique for each material and must be determined individually.

Third, the broadening effects must be considered, and as such the VB and CB locations in the presence of experimental broadening are difficult to determine. The second derivative of the spectra is utilized to unambiguously determine these edges.[29] To summarize, the core hole shift and nonequivalent site splitting provide numerical values that must be added to the nominal band gap determined from the second derivatives of the experimental spectra. These three considerations are necessary to provide accurate and reliable band gap estimations.

The *ab initio* density functional theory (DFT) calculations employ the commercially available WIEN2k software.[30] This code uses the Kohn-Sham methodology with spherical wave functions to model core orbitals, and linearized augmented plane waves (LAPW) for semicore and valence or conduction band states.[31] The exchange interaction uses the generalized gradient approximation (GGA) of Perdew-Burke-Ernzerhof.[32] We note that this approximation is known to significantly underestimate the band gap (50%–100%), but can provide good agreement with the shape of the valence and conduction bands and in turn the measured soft x-ray spectra. The effects from this core hole are modeled in the current work by including a single core hole at the atom of interest inside a $1\times1\times2$ supercell. The energy cutoff for the plane wave basis was −6.0 Ryd. A 1000 *k*-point and 100 *k*-point mesh for the unit cell and the supercell are used, respectively. The core hole shift was determined by comparing the calculated conduction energy location, including the core hole, to the conduction band energy location calculated without the core hole. The nonequivalent site splitting was determined from the core level energy eigenvalues for the N 1*s* orbital.

The x-ray diffraction (XRD) patterns indicate that atoms in the solid solution structures all exhibit the same fcc symmetry as the end members. This indicates that the substitution of Ge for Si or vice versa occurred uniformly retaining their fcc symmetry. The Fd-$3m$ spacegroup is reduced to F resulting in two tetrahedral sites and four octahedral sites for a total of six cation sites. The stoichiometry of the actual materials does not result in structures that allow for tractable DFT simulations because the concentrations are not fractions with base six (0.178 as opposed to 0.167) and would result in partial atom substitutions in the unit cell. The calculations were performed using the closest stoichiometry to the real solutions that produced ideal structures, but the stoichiometry used did not deviate more than 7% from the actual values. The lattice parameters and internal N bond parameters were chosen by interpolating the data from previous results.[21] The space group symmetry has been reduced to fcc, but other lattice choices are available to increase the symmetry in the calculation without changing the structure. The structures for γ-$(Ge_xSi_{1-x})_3N_4$ (x=0.000, 0.167, 0.333, and 1.000) retain their cubic lattices, while γ-$(Ge_xSi_{1-x})_3N_4$ (x=0.500 and 0.833) form rhombohedral lattice structures. The only assumptions used are: (1) the cations and anion sites retain fcc symmetry and (2) the tetrahedral sites are first filled with Ge atoms.

IV. RESULTS AND DISCUSSION

A. Soft x-ray spectra

The N Kα XES and N 1*s* XANES spectra are used to compare the different stoichiometries because the solid solutions and the end members all contain nitrogen in tetrahedral coordination. There is also a large number of N *p*-states in the CB and VB, making this an appropriate route to examine the electronic structure. The calculated spectra reproduce all the features seen in the experimental spectra (see Fig. 1). The small disagreement observed for N 1*s* XANES spectra is attributed to the difference between the ideal and experimental stoichiometry of the solid solutions. The three solid solution samples with stoichiometries that were the closest to the experiment samples (i.e., x=0.000, 0.347, and 1.000) exhibit the best agreement between the calculated and measured spectra. Overall, the modeling of the XES and XANES spectra with DFT calculations and the assumptions used for the structural models are appropriate for these materials.

The N Kα XES and N 1*s* XANES spectra of all samples have a similar appearance due to common local bonding environments (tetrahedral bonds with Si or Ge) and all exhibit intensive features near the Fermi level (see Fig. 1). The XES spectra consist of one strong feature *c* at ≈393–394 eV followed by two less intense features *a* and *b* positioned at 392–393 eV and 386–387 eV. The strong feature *c* in the XES spectra is due to a large amount of N *p* states at the top of the VB. The N *p* states in the VB have a large degree of hybridization with Si or Ge *s*, *p*, and *d* states and the effect of the Ge and Si neighboring atoms is seen in the N Kα XES spectra. The key difference between the XES spectra is manifested in the relative intensity of features *a* and *b* in comparison to *c*. The relative intensity of feature *c* in comparison to features *a* and *b* is greatly increased as the Si content is increased. This indicates that the nonbonding N *p* states that are situated at the top of the VB are prominent in γ-Si_3N_4 and less so in γ-Ge_3N_4.

The N *p* CB states display slight differences for the sample series (see Fig. 1). The effect of the core hole is apparent when comparing the ground state N *p*-states DOS to the corresponding XANES spectrum. The sharpness (width) of the spectral features in the XANES spectra depends on the number of nonequivalent sites within the lattice. The structures with more nonequivalent sites have broader spectral features because of the difference of the N 1*s* binding energy between the nonequivalent sites. The simulated XANES spectra all utilize a full core hole potential and agree remarkably well with the measured XANES spectra. This demonstrates that the inclusion of the core hole in XANES spectra is essential for correctly reproducing the experimental spectra. The level of agreement also confirms that

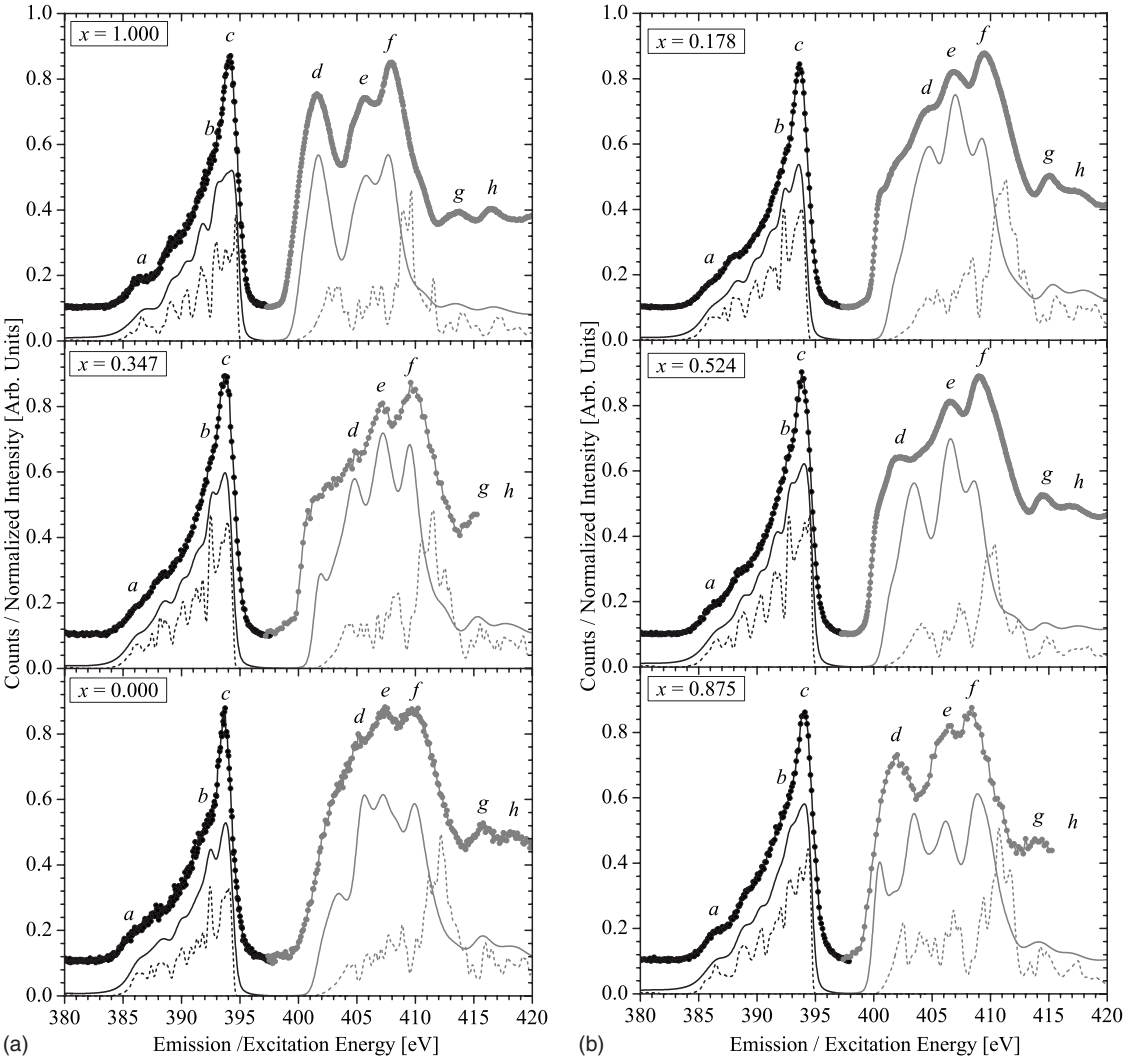

FIG. 1. The N Kα XES (in black) and N 1*s* XANES (in gray) measured spectra of γ-$(Ge_xSi_{1-x})_3N_4$ are plotted as scatter, while the corresponding calculated spectra are plotted as solid lines. The ground state N *p* DOS are shown as dashed lines and the comparison between the DOS and the calculated XANES spectra demonstrates the effect of the core hole. The DOS and simulated spectra have been shifted arbitrarily as a whole (with respect to the CB and VB) to achieve optimal peak alignment. The features discussed in the text are labeled with lower case italic lettering.

the DFT calculations successfully determine the shape of the ground state DOS.

The XANES spectra all consist of a similar three-peak structure near the Fermi level followed by a two-peak structure above 413 eV. The two features *g* and *h* at 414–415 eV and 418–419 eV are not affected by the core hole and are part of what could be considered the unperturbed N *p* CB states. The three low energy features *d*, *e* and *f* are influenced by the presence of the core hole. The sharpest features *d* and *e* near the Fermi level show the largest distortion, while feature *f* at approximately 408–410 eV feature is only shifted slightly due to the core hole. Feature *f*'s energy position decreases with an increase in Ge content, except for $x=0.178$ and 0.347 for which the band gap was predicted to remain the same or increase (see Table II). The XES energy of feature *c* (see Fig. 1) varies with Ge concentration as well. The general increase of the energy of *c* in these spectra is due the increase in binding energy of the nitrogen to cation bonds because N-Ge_4 bonds have a larger N 1*s* binding energy than N-Si_4 bonds. The position of the XES and XANES spectral features suggests that the band gap depends strongly on the stoichiometry.

B. Determining band gap and hardness

The band gaps of the γ-$(Ge,Si)_3N_4$ compounds were determined from the SXS spectra. The effect of the core hole must be taken into account all cases, the highly covalent bonds in these materials show little or no core hole shifting (see Table II). The corrected experimental values are determined by applying the corrections outlined in the experimental section (see Table II). The error attributed to the band gap is determined by two factors: the precision of the experimental spectra (this is reflected in the precision of the second derivative) and the uncertainty of calibration. The value of these errors combined is $\approx$0.20 eV and it is important to

TABLE II. The final corrected band gaps (E_g^{exp}) of the solid solutions are compared to the calculated values (E_g^{calc}) using GGA. The experimental band gap values and structural parameters are used to determine a experimental hardness estimate (H_v^{exp}), these are compared to previous hardness values determined from calculations (H_v^{calc}). Furthermore, the calculated band gaps are determined to be direct (d) or indirect (i). x refers to the experimental (x^{exp}) and simulation x^{calc} mole fraction of Ge. The approximate core hole shift (E_{ch}) is used to correct the measured band gap values to account for the presence of the core hole.

x^{calc} (%Ge)	E_g^{calc} (eV)	H_v^{calc} (GPa)	x^{exp} (%Ge)	E_{ch} (eV)	E_g^{exp} ($\pm$0.20 eV)	H_v^{exp} (GPa)
0.000	3.44[d]	30[a]	0.000	0.00	4.85	36.0 ± 9.9
0.167	3.44[d]		0.178	0.00	4.80	35.0 ± 9.7
0.333	3.56[d]	28[a]	0.347	0.15	5.00	35.6 ± 9.8
0.500	2.84[i]		0.524	0.10	4.25	25.2 ± 9.0
0.833	2.22[d]		0.875	0.05	3.65	23.6 ± 8.6
1.000	2.20[d]	18[a]	1.000	0.05	3.50	22.2 ± 8.5

[a]Reference 7.

note that because we use the second derivative to determine the VB and CB edge, the experimental broadening does not provide a significant source of error.

The hardness of covalently bonded materials has been shown to follow the empirical relationship proposed by Gilman[10] that connects hardness with the band gap and structure. This is applied to the solid solutions here and gives an estimate of the hardness tunability. The structures determined from XRD measurements[17] along with the current band gap values are used to calculate the bond modulus ($B_m = E_g / V_m$). The unknown constant ($C = 439.0 \pm 90.7$ Å^3/eV) is fit so the hardness of γ-Si_3N_4 is the experimentally measured value of 36 ± 5 GPa (Ref. 5) (see Fig. 2). The hardness values of the intermediate solid solutions are determined with the fit constant and the experimental band gaps. The error associated with the hardness is due to the uncertainty in the band gap and the proportionality constant. The structure determined from XRD did not contain a significant error. The hardness is then plotted as a function of Ge concentration showing an interesting correlation to the band gap (see Fig. 2).

These errors associated with the measured band gap values are small in comparison to the band gap value (less than 5%) and the only significant source of error is the energy calibration. The difference between the calculated and measured band gaps on average is 1.4 eV, well within the range of acceptable underestimation (50%–100%) of the band gap widely seen with the use of GGA and LDA functionals. The band gap of γ-Si_3N_4 was previously shown to be 4.3 eV[33] and 3.6 eV.[4] The value of 4.3 eV was determined with a similar method (XES and XANES) and 3.6 eV was determined using a plasmon frequency technique. The 4.3 eV band gap differs significantly for the following reasons: the Si $L_{2,3}$ are used and the spin-orbit splitting, core hole effect, and nonequivalent site splitting were not taken into account. Therefore it is not surprising that the value is much smaller than the value we have determined, since these effects will decrease the measured band gap. While there have been other band gap estimations for γ-Si_3N_4, none have rigorously included the factors accounted for here to obtain a reliable band gap value.

The measured and calculated band gap values of the spinel nitride solid solutions exhibit a similar compositional trend. The overall compositional trend of the band gap values for the solid solutions is nonlinear. However, the band gap shows a linear variation with Ge content in the range of $x = 0.333 - 1.00$ with a band gap range of 5.0–3.5 eV providing a large tunable range in the UV regime. When the relative Ge

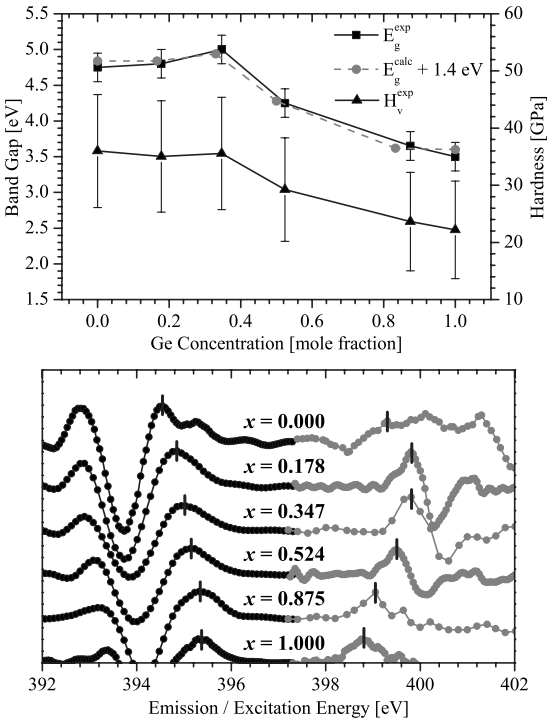

FIG. 2. The bottom panel shows the second derivative of the measured N Kα XES (black) and N 1s XANES (gray) spectra displayed in Fig. 1. The second derivative of each spectrum is calculated after the high frequency noise has been filtered out using a fast Fourier transform. The highest occupied states in the VB and the lowest unoccupied states in the CB are each labeled with a vertical line. The calculated and measured band gap values with experimental errors are displayed in the top panel. The calculated band gap values are offset vertically by the average difference between itself and the experimental values, which provides an easy comparison. The top panel also shows the determined hardness values and there is a similar trend to that of the band gap values.

concentration is smaller than 1/3 ($x \leq 1/3$), the tetrahedral sites are first filled with Ge, which increases the band gap. Conversely, when the relative Ge concentration becomes large than 1/3 ($x \geq 1/3$), the octahedral sites are then filled with Ge which decreases the band gap. This suggests that addition of the octahedral sites is possibly responsible for the decrease in the band gap in comparison to the hexagonal phases. The hardness exhibits a similar trend to the band gap values. The hardness decreases as the Ge content increases, however when relative Ge concentration is less than 1/3 ($x \leq 1/3$), the hardness only decreases slightly. The general decrease of hardness occurs because the structure becomes more open decreasing the bond strengths, but the corresponding increase in the band gap with and increase in Ge content ($x \leq 1/3$) mutes the effect. Once the octahedral site begin to fill with Ge the band gap begins to decrease with increasing Ge content, and the hardness decreases dramatically. The band gap for γ-$(Ge_xSi_{1-x})_3N_4$ has a range of 3.5–5.0 eV, while its hardness has a range of 22.2–36.0 GPa.

V. CONCLUSION

The bonding of the cation and anion sites is similar throughout the nitride spinel solid solution series. The bonding in these materials is primarily covalent and the positions of the XANES peaks are largely affected by the core hole. The energy positions of high energy XANES spectral features have a similar trend as the band gap, while the positions of the XES peaks vary in accordance with the N 1*s* binding energy. The measured band gaps of γ-$(Ge_xSi_{1-x})_3N_4$ solid solutions using SXS have a range of $3.50-5.00 \pm 0.20$ eV and the calculated band gaps using DFT calculations (GGA) have a range of 2.20–3.54 eV. The compositional trend of the band gap values agrees within experimental error if the 1.4 eV underestimation of the band gap is neglected. The trend of the hardness values is very similar to the corresponding band gap value trend and the maintained hardness for $x=1/3$ is attributed to the increase of the band gap. The band gap has a linear tunable range when $x=0$ to 1/3 and has a maintained hardness of $\approx$36 GPa. There is a larger linear band gap range when $x=1/3$ to 1, in which the hardness is significantly decreased. The solid solutions of γ-$(Ge_xSi_{1-x})_3N_4$ provide a class of wide band gap semiconductors with two tunable band gap and hardness regimes.

ACKNOWLEDGMENTS

We gratefully acknowledge the Natural Sciences and Engineering Research Council of Canada (NSERC) and the Canada Research Chair program for their support in this research. We also thank the Advanced Light Source and Canadian Light Source along with their staff for helping us to conduct this research. P.F.M. and E.B. acknowledge support from the U.K. EPSRC via Portfolio Award No. EP/D504782. P.F.M. is an EPSRC Senior Research Fellow (EP/D07357X).

*teak.boyko@usask.ca

[1] R. N. Katz, Science **208**, 841 (1980).
[2] A. Zerr, G. Miehe, G. Serghiou, M. Schwarz, E. Kroke, R. Riedel, H. Fuess, P. Kroll, and R. Boehler, Nature (London) **400**, 340 (1999).
[3] G. Serghiou, G. Miehe, O. Tschauner, A. Zerr, and R. Boehler, J. Chem. Phys. **111**, 4659 (1999).
[4] R. G. Egdell, V. E. Henrich, R. Bowdler, and T. Sekine, J. Appl. Phys. **94**, 6611 (2003).
[5] A. Zerr, M. Kempf, M. Schwarz, E. Kroke, M. Göken, and R. Riedel, J. Am. Ceram. Soc. **85**, 86 (2002).
[6] S.-D. Mo, L. Ouyang, W. Y. Ching, I. Tanaka, Y. Koyama, and R. Riedel, Phys. Rev. Lett. **83**, 5046 (1999).
[7] J. Dong, J. Deslippe, O. F. Sankey, E. Soignard, and P. F. McMillan, Phys. Rev. B **67**, 094104 (2003).
[8] J. Dong, O. F. Sankey, S. K. Deb, G. Wolf, and P. F. McMillan, Phys. Rev. B **61**, 11979 (2000).
[9] K. Maeda, N. Saito, D. Lu, Y. Inoue, and K. Domen, J. Phys. Chem. C **111**, 4749 (2007).
[10] J. J. Gilman, J. Phys. D: Appl. Phys. **41**, 074020 (2008).
[11] W. Y. Ching, L. Ouyang, and J. D. Gale, Phys. Rev. B **61**, 8696 (2000).
[12] S. Ogata, N. Hirosaki, C. Kocer, and Y. Shibutani, Acta Mater. **52**, 233 (2004).
[13] Y. H. Duan, K. M. Zhang, and X. D. Xie, Phys. Status Solidi B **200**, 499 (1997).
[14] Y. M. Li, M. B. Kruger, J. H. Nguyen, W. A. Caldwell, and R. Jeanloz, Solid State Commun. **103**, 107 (1997).
[15] J. C. Hay, E. Y. Sun, G. M. Pharr, P. F. Becher, and K. B. Alexander, J. Am. Ceram. Soc. **81**, 2661 (1998).
[16] R. A. Andrievski, Int. J. Refract. Met. Hard. Mater. **19**, 447 (2001).
[17] E. Soignard, P. F. McMillan, C. Hejny, and K. Leinenweber, J. Solid State Chem. **177**, 299 (2004).
[18] E. Soignard, M. Somayazulu, J. J. Dong, O. F. Sankey, and P. F. McMillan, J. Phys.: Condens. Matter, **13**, 557 (2001).
[19] W. Y. Ching, S.-D. Mo, I. Tanaka, and M. Yoshiya, Phys. Rev. B **63**, 064102 (2001).
[20] K. Leinenweber, M. O'Keeffe, M. Somayazulu, H. Hubert, P. F. McMillan, and G. H. Wolf, Chem.-Eur. J. **5**, 3076 (1999).
[21] E. Soignard, P. F. McMillan, and K. Leinenweber, Chem. Mater. **16**, 5344 (2004).
[22] T. Regier, J. Krochak, T. K. Sham, Y. F. Hu, J. Thompson, and R. I. R. Blyth, Nucl. Instrum. Methods Phys. Res. A **582**, 93 (2007).
[23] J. J. Jia, T. A. Callcott, J. Yurkas, A. W. Ellis, F. J. Himpsel, M. G. Samant, J. Stöhr, D. L. Ederer, J. A. Carlisle, E. A. Hudson, L. J. Terminello, D. K. Shuh, and R. C. C. Perera, Rev. Sci. Instrum. **66**, 1394 (1995).
[24] M. O. Krause and J. H. Oliver, J. Phys. Chem. Ref. Data **8**, 329 (1979).
[25] D. A. Goodings and R. Harris, J. Phys. Pt. C: Sol. Stat. Phys. **2**, 1808 (1969).
[26] T. Mizoguchi, I. Tanaka, S.-P. Gao, and C. J. Pickard, J. Phys,:

Condens. Matter **21**, 104204 (2009).
[27] U. von Barth and G. Grossmann, Phys. Rev. B **25**, 5150 (1982).
[28] W. Y. Ching and P. Rulis, J. Phys.: Condens. Matter **21**, 104202 (2009).
[29] E. Z. Kurmaev, R. G. Wilks, A. Moewes, L. D. Finkelstein, S. N. Shamin, and J. Kuneš, Phys. Rev. B **77**, 165127 (2008).
[30] M. Schwarz, G. Miehe, A. Zerr, E. Kroke, B. Poe, H. Fuess, and R. Riedel, Adv. Mater. **12**, 883 (2000).
[31] K. Schwarz, P. Blaha, and G. K. H. Madsen, Comp. Phys. Comm. **147**, 71 (2002).
[32] J. P. Perdew, K. Burke, and M. Ernzerhof, Phys. Rev. Lett. **77**, 3865 (1996).
[33] S. Leitch, A. Moewes, L. Ouyang, W. Y. Ching, and T. Sekine, J. Phys.: Condens. Matter **16**, 6469 (2004).